Microstreaming generated by two acoustically induced gas bubbles

Alexander A. Doinikov[1,†] and Ayache Bouakaz[1]

[1]INSERM U930, Université François Rabelais, 10 Boulevard Tonnellé, BP 3223,
37032 Tours CEDEX 1, France

A theory is developed that describes microstreaming generated by two interacting gas bubbles in an acoustic field. The theory is used in numerical simulations to compare the characteristics of acoustic microstreaming at different frequencies, separation distances between the bubbles and bubble sizes. It is shown that the interaction of the bubbles leads to a considerable increase in the intensity of the velocity and stress fields of acoustic microstreaming if the bubbles are driven near the resonance frequencies that they have in the presence of each other. Patterns of streamlines for different situations are presented.

Key words: bubble dynamics, cavitation, drops and bubbles

1. Introduction

Vortical microstreaming plays an important role in many technical and medical applications based on the physico-chemical action of acoustically excited bubbles on objects immersed in a liquid. Ultrasonic cleaning, intensification of heat and mass exchange, stimulation of chemical reactions, haemolysis, sonothrombolysis and sonoporation are examples. The history of these applications from the 1950s up to the present can be traced through papers by Kolb & Nyborg (1956), Elder (1959), Nyborg (1965, 1978), Rooney (1970, 1972), Lighthill (1978), Liu *et al.* (2002), Wu (2002), Tho, Manasseh & Ooi (2007), Wu & Nyborg (2008), Collis *et al.* (2010) and Wang, Jalikop & Hilgenfeldt (2012). Theoretical studies on bubble-induced microstreaming were performed by Nyborg (1958), Davidson & Riley (1971), Wu & Du (1997), Longuet-Higgins (1998), Maksimov (2007), Liu & Wu (2009) and Doinikov & Bouakaz (2010*a*,*b*, 2014). The results of these studies are described in our recent paper (Doinikov & Bouakaz 2014). All the studies consider a single bubble, whereas in most practical situations one has to deal with bubble clusters. In this connection, a question arises as to how bubble interactions affect the behaviour of acoustic microstreaming.

The purpose of the present study is to develop a theory that describes acoustic microstreaming in the case of two interacting bubbles and to reveal how the interaction of the bubbles changes the characteristics of acoustic microstreaming. The proposed theory is a generalization of the calculations made in our previous paper (Doinikov &
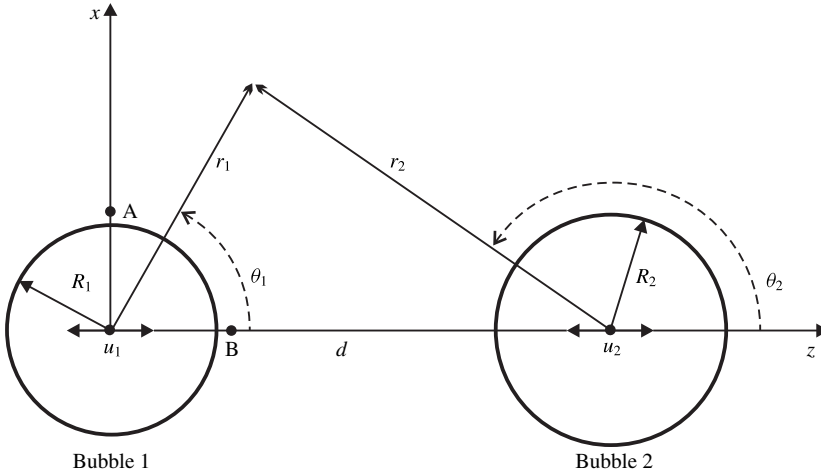
† Email address for correspondence: doinikov@bsu.by

FIGURE 1. Geometry of the problem.

Bouakaz 2014) where the interaction of a real bubble with a mirror bubble was used to describe the effect of a distant rigid wall on microstreaming generated around the real bubble. In the present paper, both bubbles are considered to be real, which means that they can be of different sizes and their oscillations are not mirror-like.

2. Theory

Consider two spherical gas bubbles suspended in a viscous liquid and undergoing radial and translational oscillations in response to an imposed acoustic pressure field (see figure 1). In order to make the problem amenable to analytical solution, we introduce simplifying assumptions. The distance d between the equilibrium centres of the bubbles is assumed to be large compared to the equilibrium bubble radii R_{10} and R_{20}, which allows one to use R_{10}/d and R_{20}/d as small parameters. The translational oscillation is assumed to be executed along the line connecting the equilibrium centres of the bubbles, which makes the problem axisymmetric. The sound wavelength is assumed to be much larger than the bubble radii and d, which allows one to consider the liquid as incompressible and to describe its motion by the following equations:

$$\nabla \cdot \boldsymbol{v} = 0, \tag{2.1}$$

$$\rho \frac{\partial \boldsymbol{v}}{\partial t} + \rho (\boldsymbol{v} \cdot \nabla) \boldsymbol{v} = \eta \Delta \boldsymbol{v} - \nabla p, \tag{2.2}$$

where $\boldsymbol{v}$ is the liquid velocity, ρ is the liquid density, η is the dynamic liquid viscosity and p is the liquid pressure.

To describe the scattered fields produced by the bubbles, we introduce two spherical coordinate systems $(r_j, \theta_j, \varepsilon_j)$, $j = 1, 2$, originated at the equilibrium centres of the bubbles.

2.1. *Incident field*

The incompressibility of the liquid implies that the velocity potential of the incident acoustic wave can be taken as $\varphi_I = A \exp(-i\omega t)$, where A is the amplitude and ω is the

angular frequency. This means that the dominant factor is pressure pulsation created by the incident wave in the liquid, whereas the translational motion of the liquid generated by the incident wave is negligible. If, however, we neglect this motion, our results will not be able to provide going to the limiting case of a single bubble in an infinite liquid ($R_{j0}/d \to 0$) because, in this case, it is the liquid translation created by the incident wave that causes the translation motion of the bubble. In order to include this effect, we use the following approximation. The velocity potential of the incident wave, which is assumed to propagate along the centreline of the bubbles, can be written as $\varphi_I = A\zeta(z)\exp(-i\omega t)$, where the function $\zeta(z)$ is a solution to the Helmholtz equation. For example, in the case of a plane travelling wave, $\zeta(z) = \exp(ikz)$, where $k = \omega/c$ is the wavenumber and c is the speed of sound in the liquid. Since the sizes of the bubbles are assumed to be much smaller than the wavelength, we can restrict ourselves to the leading terms in the expansion of $\zeta(z)$ in a Taylor series at the bubble centres. That is, for bubble 1, we take the expansion of $\zeta(z)$ at the point $z = 0$ considering the value of z to be small compared to the wavelength; and for bubble 2, we take the expansion of $\zeta(z)$ at the point $z = d$ considering $z - d$ to be small compared to the wavelength. As a result, the incident velocity potentials for bubbles 1 and 2 are written as

$$\varphi_{I1} = Ae^{-i\omega t}(1 + \xi_1 z), \quad \varphi_{I2} = Ae^{-i\omega t}[1 + \xi_2(z - d)], \quad (2.3a,b)$$

where ξ_1 and ξ_2 are constants that are determined by the type of the incident wave. In the case of a plane travelling wave, $\xi_1 = \xi_2 = ik$. The pressure and velocity fields created by the incident wave at the positions of the bubbles are given by

$$p_{I1} = -\rho\frac{\partial\varphi_{I1}}{\partial t} = i\omega\rho Ae^{-i\omega t}(1 + \xi_1 z), \quad p_{I2} = -\rho\frac{\partial\varphi_{I2}}{\partial t} = i\omega\rho Ae^{-i\omega t}[1 + \xi_2(z - d)], \quad (2.4a,b)$$

$$\boldsymbol{v}_{I1} = \nabla\varphi_{I1} = \boldsymbol{e}_z\xi_1 Ae^{-i\omega t}, \quad \boldsymbol{v}_{I2} = \nabla\varphi_{I2} = \boldsymbol{e}_z\xi_2 Ae^{-i\omega t}, \quad (2.5a,b)$$

where $\boldsymbol{e}_z$ is the unit vector along the axis z. Equations (2.3)–(2.5) allow for the velocity field created by the incident wave in the ambient liquid.

2.2. *Linear scattered field*

Linearizing (2.1) and (2.2) yields

$$\nabla \cdot \boldsymbol{v}_L = 0, \quad (2.6)$$

$$\rho\frac{\partial\boldsymbol{v}_L}{\partial t} = \eta\Delta\boldsymbol{v}_L - \nabla p_L, \quad (2.7)$$

where the subscript L denotes that the quantities are taken in the linear approximation, i.e. accurate to first order in the acoustic pressure amplitude. The velocity $\boldsymbol{v}_L$ can be represented as

$$\boldsymbol{v}_L = \nabla\varphi + \nabla \times \boldsymbol{\psi}, \quad (2.8)$$

where φ and $\boldsymbol{\psi}$ are the linear scalar and vorticity velocity potentials. Substituting (2.8) into (2.6) and (2.7) and taking into consideration that the time dependence is $\exp(-i\omega t)$, one obtains the equations

$$\Delta\varphi = 0, \quad (2.9)$$

$$(\Delta + k_v^2)\boldsymbol{\psi} = 0, \quad (2.10)$$

where $k_v = (1 + \mathrm{i})/\delta_v$ is the viscous wavenumber, $\delta_v = \sqrt{2\nu/\omega}$ is the viscous penetration depth and $\nu = \eta/\rho$ is the kinematic liquid viscosity.

Considering that we have two bubbles and that they execute radial and translational motions, the scalar potential satisfying (2.9) can be written as

$$\varphi = \varphi_1 + \varphi_2, \tag{2.11}$$

where φ_j, the scalar potential of the jth bubble, is given by

$$\varphi_j = A\mathrm{e}^{-\mathrm{i}\omega t}\left[\frac{a_j R_{j0}}{r_j} + b_j\left(\frac{R_{j0}}{r_j}\right)^2\cos\theta_j\right], \tag{2.12}$$

with R_{j0} the equilibrium radius of the jth bubble and a_j and b_j dimensionless constants to be determined by the boundary conditions at the surfaces of the bubbles. It should be emphasized that, for each of the bubbles, both potentials φ_1 and φ_2, since they appear in the total potential, are involved in enforcing the boundary condition at the bubble surface.

The vorticity potential satisfying (2.10) can be written as

$$\boldsymbol{\psi} = \boldsymbol{\psi}_1 + \boldsymbol{\psi}_2, \tag{2.13}$$

where $\boldsymbol{\psi}_j$, the vorticity potential of the jth bubble, is given by the following equation (Doinikov & Bouakaz 2014):

$$\boldsymbol{\psi}_j = A\mathrm{e}^{-\mathrm{i}\omega t}c_j h_1^{(1)}(k_v r_j)\sin\theta_j\,\boldsymbol{e}_{\varepsilon j}. \tag{2.14}$$

In the latter, c_j is a dimensionless constant, $h_1^{(1)}(z) = -\exp(\mathrm{i}z)(1/z + \mathrm{i}/z^2)$ is the spherical Hankel function of the first kind (Abramowitz & Stegun 1972) and $\boldsymbol{e}_{\varepsilon j}$ is the unit azimuth vector of the spherical coordinate system related to the jth bubble.

From (2.12) and (2.14), one finds the components of (2.8) to be

$$\nabla\varphi_j = -A\mathrm{e}^{-\mathrm{i}\omega t}\left[\boldsymbol{e}_{rj}\left(\frac{a_j R_{j0}}{r_j^2} + \frac{2b_j R_{j0}^2}{r_j^3}\cos\theta_j\right) + \boldsymbol{e}_{\theta j}\frac{b_j R_{j0}^2}{r_j^3}\sin\theta_j\right], \tag{2.15}$$

$$\nabla\times\boldsymbol{\psi}_j = A\mathrm{e}^{-\mathrm{i}\omega t}\frac{c_j}{r_j}[2\boldsymbol{e}_{rj}h_1^{(1)}(k_v r_j)\cos\theta_j - \boldsymbol{e}_{\theta j}(h_1^{(1)}(k_v r_j) + k_v r_j h_1^{(1)\prime}(k_v r_j))\sin\theta_j], \tag{2.16}$$

where $h_1^{(1)\prime}(z) = \mathrm{d}h_1^{(1)}(z)/\mathrm{d}z$.

To calculate the unknown constants in (2.15) and (2.16), the boundary conditions for normal velocity, normal stress and tangential stress at the bubble surface are applied. The boundary condition for the normal velocity at the surface of the jth bubble is given by

$$\boldsymbol{e}_{rj}\cdot(\boldsymbol{v}_{Ij} + \boldsymbol{v}_L) = \dot{R}_j + u_j\cos\theta_j \quad \text{at } r_j = R_{j0}, \tag{2.17}$$

where R_j and u_j are the instantaneous radius and the translational velocity of the jth bubble (see figure 1) and $\dot{R}_j = \mathrm{d}R_j/\mathrm{d}t$. Substituting (2.5), (2.15) and (2.16) into (2.17) and keeping terms up to second order in the small parameter R_{j0}/d, one obtains

$$a_j A\mathrm{e}^{-\mathrm{i}\omega t} = -R_{j0}\dot{R}_j, \tag{2.18}$$

$$u_j = \frac{A \exp(-\mathrm{i}\omega t)}{R_{j0}} \left(R_{j0}\xi_j + (-1)^{j+1}\frac{R_{10}R_{20}}{d^2}a_{3-j} - 2b_j + 2c_j h_1^{(1)}(\alpha_j) \right), \qquad (2.19)$$

where $\alpha_j = k_v R_{j0}$. Note that these equations were calculated assuming a_j to be of zeroth order in R_{j0}/d, and b_j and c_j to be of second order in R_{j0}/d. We will see below that this is so indeed; see also Doinikov & Bouakaz (2014).

The boundary condition for the normal stress at the surface of the jth bubble is given by

$$P_{gj}\left(\frac{R_{j0}}{R_j}\right)^{3\gamma} = p_{Ij} + p_L + P_0 + \frac{2\sigma}{R_j} - 2\eta\frac{\partial v_{rj}}{\partial r_j} \quad \text{at } r_j = R_{j0}, \qquad (2.20)$$

where P_{gj} is the equilibrium pressure of the gas inside the jth bubble, γ is the ratio of specific heats of the gas, P_0 is the hydrostatic pressure in the liquid, σ is the surface tension, $v_{rj} = \boldsymbol{e}_{rj} \cdot (\boldsymbol{v}_{Ij} + \boldsymbol{v}_L)$ and the scattered pressure p_L is equal to $-\rho\partial\varphi/\partial t$. Linearizing (2.20) and using (2.4), (2.5), (2.12), (2.15), (2.16) and (2.18), with accuracy up to $(R_{j0}/d)^2$, one obtains the following equations:

$$P_{gj} = P_0 + \frac{2\sigma}{R_{j0}}, \qquad (2.21)$$

$$\left(\frac{\omega_j^2}{\omega^2} - 1 - \mathrm{i}\delta_j\right)a_j - \frac{R_{3-j0}}{d}a_{3-j} = 1, \qquad (2.22)$$

$$(12 - \alpha_j^2)b_j + 4(\alpha_j h_1^{(1)\prime}(\alpha_j) - h_1^{(1)}(\alpha_j))c_j = \alpha_j^2\left((-1)^{j+1}\frac{R_{10}R_{20}}{d^2}a_{3-j} + R_{j0}\xi_j\right), \qquad (2.23)$$

where ω_j is the angular resonance frequency of the jth bubble in the absence of the other bubble, given by

$$\omega_j = \frac{1}{R_{j0}}\left(\frac{3\gamma P_{gj}}{\rho} - \frac{2\sigma}{\rho R_{j0}}\right)^{1/2}, \qquad (2.24)$$

and δ_j is the viscous damping constant, defined as

$$\delta_j = \frac{4\nu}{\omega R_{j0}^2}. \qquad (2.25)$$

From (2.22) it follows that

$$a_j = \frac{1}{D}\left(\frac{\omega_{3-j}^2}{\omega^2} - 1 - \mathrm{i}\delta_{3-j} + \frac{R_{3-j0}}{d}\right), \qquad (2.26)$$

where

$$D = \left(\frac{\omega_1^2}{\omega^2} - 1 - \mathrm{i}\delta_1\right)\left(\frac{\omega_2^2}{\omega^2} - 1 - \mathrm{i}\delta_2\right) - \frac{R_{10}R_{20}}{d^2}. \qquad (2.27)$$

To complete the calculation of the constants, the boundary condition for the tangential stress $\sigma_{r\theta}$ is used:

$$\sigma_{r\theta} = \eta\left(\frac{1}{r_j}\frac{\partial v_{rj}}{\partial\theta_j} + \frac{\partial v_{\theta j}}{\partial r_j} - \frac{v_{\theta j}}{r_j}\right) = 0 \quad \text{at } r_j = R_{j0}, \qquad (2.28)$$

where $v_{\theta j} = \boldsymbol{e}_{\theta j} \cdot (\boldsymbol{v}_{Ij} + \boldsymbol{v}_L)$. On substitution of (2.5), (2.15) and (2.16), equation (2.28) gives

$$6b_j = \alpha_j^2 h_1^{(1)''}(\alpha_j)c_j. \tag{2.29}$$

Solving (2.23) and (2.29) for b_j and c_j, one obtains

$$b_j = \frac{\alpha_j^3 + 3i\alpha_j^2 - 6\alpha_j - 6i}{18i + 18\alpha_j - 3i\alpha_j^2 - \alpha_j^3}\left((-1)^{j+1}\frac{R_{10}R_{20}}{d^2}a_{3-j} + R_{j0}\xi_j\right), \tag{2.30}$$

$$c_j = \frac{6\alpha_j^2 \exp(-i\alpha_j)}{18i + 18\alpha_j - 3i\alpha_j^2 - \alpha_j^3}\left((-1)^{j+1}\frac{R_{10}R_{20}}{d^2}a_{3-j} + R_{j0}\xi_j\right). \tag{2.31}$$

Substitution of (2.30) and (2.31) into (2.19) yields

$$u_j = \frac{3A\exp(-i\omega t)}{R_{j0}}\frac{6i + 6\alpha_j - 3i\alpha_j^2 - \alpha_j^3}{18i + 18\alpha_j - 3i\alpha_j^2 - \alpha_j^3}\left((-1)^{j+1}\frac{R_{10}R_{20}}{d^2}a_{3-j} + R_{j0}\xi_j\right). \tag{2.32}$$

2.3. *Acoustic streaming*

By averaging (2.1) and (2.2) over time and keeping up to the second order in the acoustic pressure amplitude, one obtains the equations of acoustic streaming:

$$\boldsymbol{\nabla}\cdot\boldsymbol{V} = 0, \tag{2.33}$$
$$\eta\Delta\boldsymbol{V} - \boldsymbol{\nabla}P = \rho\langle(\boldsymbol{v}_L\cdot\boldsymbol{\nabla})\boldsymbol{v}_L\rangle. \tag{2.34}$$

Here $\langle\ \rangle$ means the time average, and $\boldsymbol{V}$ and P are the velocity and the pressure fields of acoustic streaming. To satisfy (2.33), $\boldsymbol{V}$ is taken as

$$\boldsymbol{V} = \boldsymbol{\nabla}\times\boldsymbol{\Psi}. \tag{2.35}$$

Substituting (2.35) into (2.34), applying the curl operator, using (2.8) and (2.10) and keeping up to $(R_{j0}/d)^2$, one has

$$\Delta^2\boldsymbol{\Psi} = -\frac{1}{\nu}\boldsymbol{\nabla}\times\langle(\boldsymbol{v}_L\cdot\boldsymbol{\nabla})\boldsymbol{v}_L\rangle = \frac{1}{2\nu}\text{Re}\{k_v^2\boldsymbol{\nabla}\times(\boldsymbol{\nabla}\varphi^*\times\boldsymbol{\psi})\}, \tag{2.36}$$

where Re means 'the real part of' and the asterisk indicates the complex conjugate.
The potential $\boldsymbol{\Psi}$ can be written as

$$\boldsymbol{\Psi} = \boldsymbol{\Psi}_1 + \boldsymbol{\Psi}_2, \tag{2.37}$$

where $\boldsymbol{\Psi}_j$, with accuracy up to $(R_{j0}/d)^2$, is calculated by

$$\Delta^2\boldsymbol{\Psi}_j = \frac{1}{2\nu}\text{Re}\{k_v^2\boldsymbol{\nabla}\times(\boldsymbol{\nabla}\varphi_j^*\times\boldsymbol{\psi}_j)\}. \tag{2.38}$$

Substitution of (2.14), (2.15) and $h_1^{(1)}(k_v r_j)$ into (2.38) yields

$$\Delta^2\boldsymbol{\Psi}_j = \frac{|A|^2 R_{j0}}{2\nu}\frac{\sin\theta_j}{r_j^5}\boldsymbol{e}_{\varepsilon j}\text{Re}\{a_j^* c_j\exp(ik_v r_j)(3i + 3k_v r_j - ik_v^2 r_j^2)\}. \tag{2.39}$$
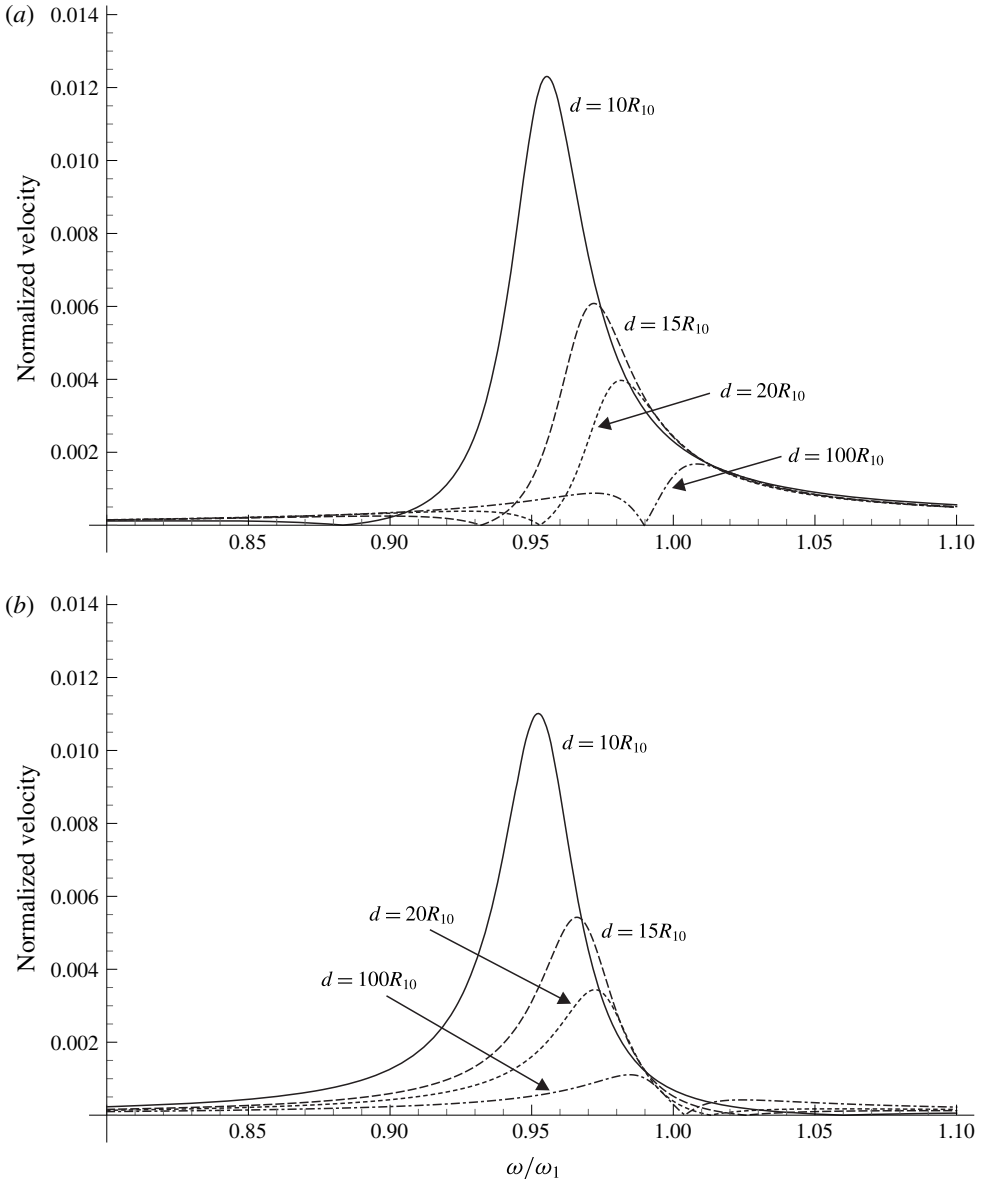
FIGURE 2. Magnitude of the streaming velocity versus driving frequency for different values of the separation distance at two representative spatial points shown in figure 1: (*a*) point A and (*b*) point B. Calculations were made for bubbles of equal size, $R_{10} = R_{20} = 5$ μm, subjected to a plane travelling wave.

It has been shown by Doinikov & Bouakaz (2014) that the solution to (2.39) can be written as

$$\boldsymbol{\Psi}_j = \frac{|A|^2 R_{j0}}{2\nu} \sin\theta_j \, \boldsymbol{e}_{\varepsilon j} \, \mathrm{Re}\{a_j^* c_j G_j(r_j)\}, \tag{2.40}$$

where $G_j(r_j)$ is given by

$$G_j(r_j) = A_{1j}(r_j)r_j^{-2} + A_{2j}(r_j) + A_{3j}(r_j)r_j + A_{4j}(r_1)r_j^3, \tag{2.41}$$
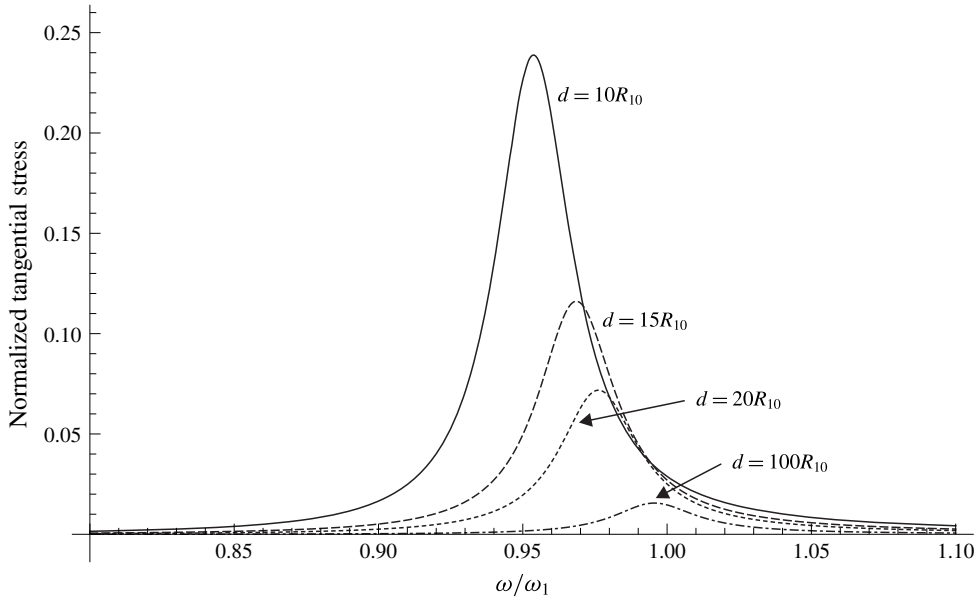
FIGURE 3. Magnitude of the tangential stress versus driving frequency for different values of the separation distance. The stress is calculated at point A. Parameters are as in figure 2.
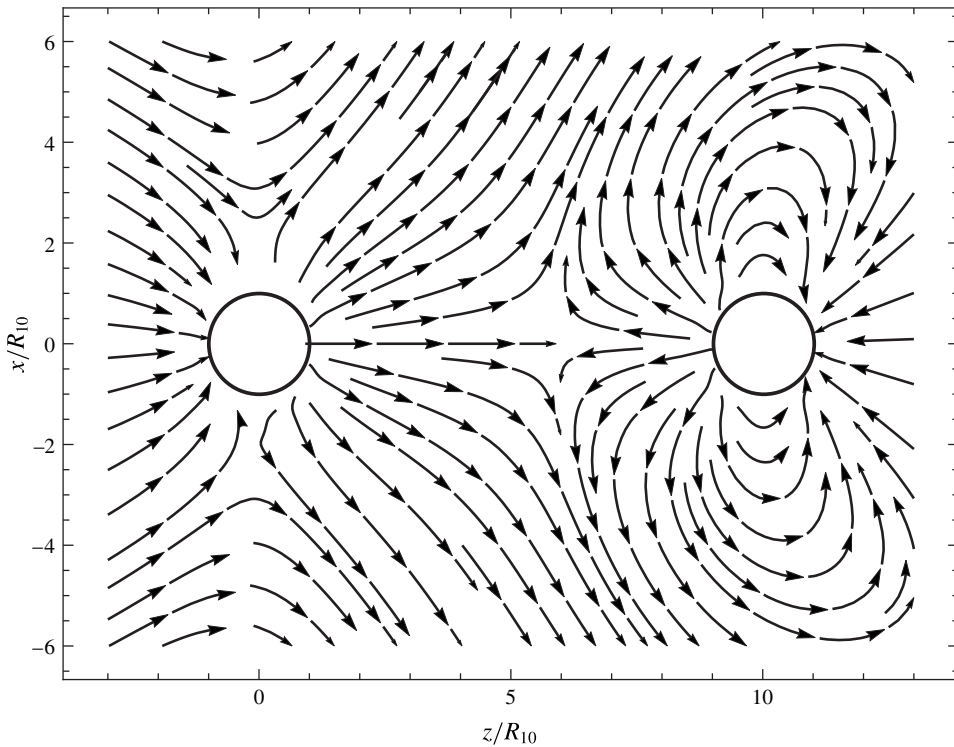
FIGURE 4. Streamlines in the case shown in figure 2 at $d = 10R_{10}$ and $\omega = 0.95\omega_1$.

in which the functions $A_{nj}(r_j)$ are calculated by

$$A_{1j}(r_j) = B_{1j} - \frac{8 - 5\mathrm{i}k_v r_j - k_v^2 r_j^2}{30 k_v} \exp(\mathrm{i}k_v r_j), \tag{2.42}$$

$$
\begin{aligned}
A_{2j}(r_j) &= B_{2j} - \frac{k_v}{6} \exp(\mathrm{i}k_v r_j) + \frac{\mathrm{i}}{2} \int_{R_{j0}}^{r_j} r^{-2} \exp(\mathrm{i}k_v r)(1 - \mathrm{i}k_v r)\,\mathrm{d}r \\
&= B_{2j} + \frac{\mathrm{i}}{2R_{j0}} \exp(\mathrm{i}\alpha_j) - \frac{3\mathrm{i} + k_v r_j}{6 r_j} \exp(\mathrm{i}k_v r_j),
\end{aligned}
\tag{2.43}
$$

$$A_{3j}(r_j) = B_{3j} - \frac{\mathrm{i}}{6} \int_{R_{j0}}^{r_j} r^{-3} \exp(\mathrm{i}k_v r)(3 - 3\mathrm{i}k_v r - k_v^2 r^2)\,\mathrm{d}r, \tag{2.44}$$

$$A_{4j}(r_j) = B_{4j} + \frac{\mathrm{i}}{30} \int_{R_{j0}}^{r_j} r^{-5} \exp(\mathrm{i}k_v r)(3 - 3\mathrm{i}k_v r - k_v^2 r^2)\,\mathrm{d}r, \tag{2.45}$$

where B_{nj} are constants. From the condition that $V \to 0$ as $r_j \to \infty$, one has

$$
\begin{aligned}
B_{3j} &= \frac{\mathrm{i}}{6} \int_{R_{j0}}^{\infty} r^{-3} \exp(\mathrm{i}k_v r)(3 - 3\mathrm{i}k_v r - k_v^2 r^2)\,\mathrm{d}r \\
&= \frac{\mathrm{i}}{12 R_{j0}^2}[3(1 - \mathrm{i}\alpha_j) \exp(\mathrm{i}\alpha_j) + \alpha_j^2 E_1(-\mathrm{i}\alpha_j)],
\end{aligned}
\tag{2.46}
$$

$$
\begin{aligned}
B_{4j} &= -\frac{\mathrm{i}}{30} \int_{R_{j0}}^{\infty} r^{-5} \exp(\mathrm{i}k_v r)(3 - 3\mathrm{i}k_v r - k_v^2 r^2)\,\mathrm{d}r \\
&= -\frac{\mathrm{i}}{240 R_{j0}^4}[(6 - 6\mathrm{i}\alpha_j - \alpha_j^2 - \mathrm{i}\alpha_j^3) \exp(\mathrm{i}\alpha_j) + \alpha_j^4 E_1(-\mathrm{i}\alpha_j)],
\end{aligned}
\tag{2.47}
$$

where $E_1(z)$ is the exponential integral of the first order (Abramowitz & Stegun 1972). Substitution of (2.46) and (2.47) into (2.44) and (2.45) gives

$$A_{3j}(r_j) = \frac{\mathrm{i}}{12 r_j^2}[3(1 - \mathrm{i}k_v r_j) \exp(\mathrm{i}k_v r_j) + k_v^2 r_j^2 E_1(-\mathrm{i}k_v r_j)], \tag{2.48}$$

$$A_{4j}(r_j) = -\frac{\mathrm{i}}{240 r_j^4}[(6 - 6\mathrm{i}k_v r_j - k_v^2 r_j^2 - \mathrm{i}k_v^3 r_j^3) \exp(\mathrm{i}k_v r_j) + k_v^4 r_j^4 E_1(-\mathrm{i}k_v r_j)]. \tag{2.49}$$

To find B_{1j}, the boundary condition for the tangential stress produced by the acoustic streaming at the bubble surface is applied (Doinikov & Bouakaz 2014). For the jth bubble, this condition is given by

$$T_{r\theta} + \langle (z_j \mathbf{e}_z + R_j \mathbf{e}_{rj}) \cdot \nabla \sigma_{r\theta} \rangle = 0 \quad \text{at } r_j = R_{j0}, \tag{2.50}$$

where z_j is the displacement of the centre of the jth bubble along the axis z, defined as $\mathrm{d}z_j/\mathrm{d}t = u_j$, $\sigma_{r\theta}$ is the linear tangential stress given by (2.28) and $T_{r\theta}$ denotes the tangential stress produced by the acoustic streaming, which is calculated by

$$T_{r\theta} = \eta \left(\frac{1}{r_j} \frac{\partial V_{rj}}{\partial \theta_j} + \frac{\partial V_{\theta j}}{\partial r_j} - \frac{V_{\theta j}}{r_j} \right), \tag{2.51}$$

where $V_{rj} = e_{rj} \cdot V$ and $V_{\theta j} = e_{\theta j} \cdot V$ are the radial and tangential components of V in the coordinates of the jth bubble. As follows from (2.35), (2.37) and (2.40), V is given by

$$V = V_1 + V_2, \tag{2.52}$$

where

$$V_j = \nabla \times \Psi_j = \frac{|A|^2 R_{j0}}{2\nu r_j} \operatorname{Re}\{a_j^* c_j [2G_j(r_j)\cos\theta_j\, e_{rj} - (G_j(r_j) + r_j G_j'(r_j))\sin\theta_j\, e_{\theta j}]\}, \tag{2.53}$$

with $G_j'(r_j) = \mathrm{d}G_j/\mathrm{d}r_j$. Accordingly, $T_{r\theta}$ can be represented as

$$T_{r\theta} = T_1 + T_2, \tag{2.54}$$

where T_j is calculated by substituting V_j into (2.51), which results in

$$T_j = -\tfrac{1}{2}\rho|A|^2 R_{j0}\sin\theta_j \operatorname{Re}\{a_j^* c_j G_j''(r_j)\}. \tag{2.55}$$

Substituting (2.54) and (2.55) into (2.50) and using (2.18), (2.28), (2.32) and (2.41), with accuracy up to $(R_{j0}/d)^2$, one gets

$$B_{1j} = \frac{8 - \alpha_j^2}{30 k_v}\exp(\mathrm{i}\alpha_j) - R_{j0}^5 B_{4j}. \tag{2.56}$$

The constant B_{2j} is found from the boundary condition for the normal velocity of the acoustic streaming, which is given by

$$V_{rj} + e_{rj} \cdot \langle[(z_j e_z + R_j e_{rj}) \cdot \nabla]v_L\rangle = 0 \quad \text{at } r_j = R_{j0}. \tag{2.57}$$

Calculating V_{rj} by (2.52) and (2.53), substituting it along with the linear solutions into (2.57) and using (2.41), one finds, with accuracy up to $(R_{j0}/d)^2$,

$$B_{2j} = \frac{18\mathrm{i} + 18\alpha_j - 6\mathrm{i}\alpha_j^2 - \mathrm{i}\alpha_j^4 + \alpha_j^5}{6\alpha_j^4 R_{j0}}\exp(\mathrm{i}\alpha_j) - R_{j0}B_{3j}. \tag{2.58}$$

It is also useful to calculate expressions for the derivatives $G_j'(r_j)$ and $G_j''(r_j)$ which appear in (2.53) and (2.55). The result is

$$G_j'(r_j) = -2r_j^{-3}A_{1j}(r_j) + A_{3j}(r_j) + 3r_j^2 A_{4j}(r_j), \tag{2.59}$$
$$G_j''(r_j) = 6r_j^{-4}A_{1j}(r_j) + 6r_j A_{4j}(r_j). \tag{2.60}$$

To sum up, the velocity and stress fields generated by the acoustic streaming are given by (2.52)–(2.55). The quantities appearing in these equations are calculated by (2.41)–(2.43), (2.46)–(2.49), (2.56) and (2.58)–(2.60).
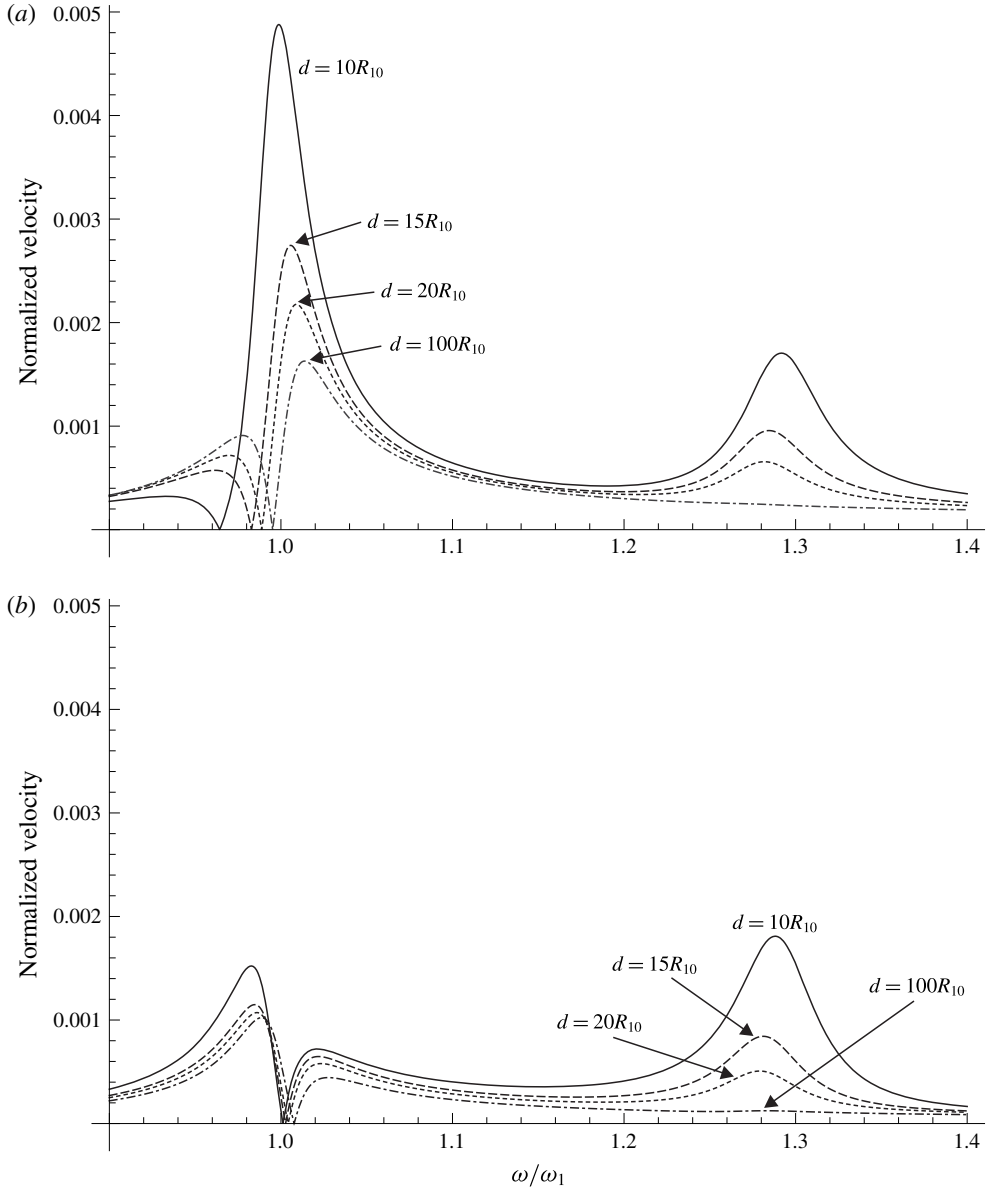
FIGURE 5. Streaming velocity for $R_{10} = 5$ μm and $R_{20} = 4$ μm: (*a*) point A and (*b*) point B. The other parameters are as in figure 2.

2.4. *Lagrangian streaming*

The Lagrangian streaming velocity is calculated by

$$V_L = V + V_S, \tag{2.61}$$

where V_S is the Stokes drift velocity defined as (Longuet-Higgins 1998)

$$V_S = \left\langle \int v_L \, dt \cdot \nabla v_L \right\rangle = \frac{1}{2\omega} \operatorname{Re}\{i(v_L \cdot \nabla)v_L^*\}. \tag{2.62}$$
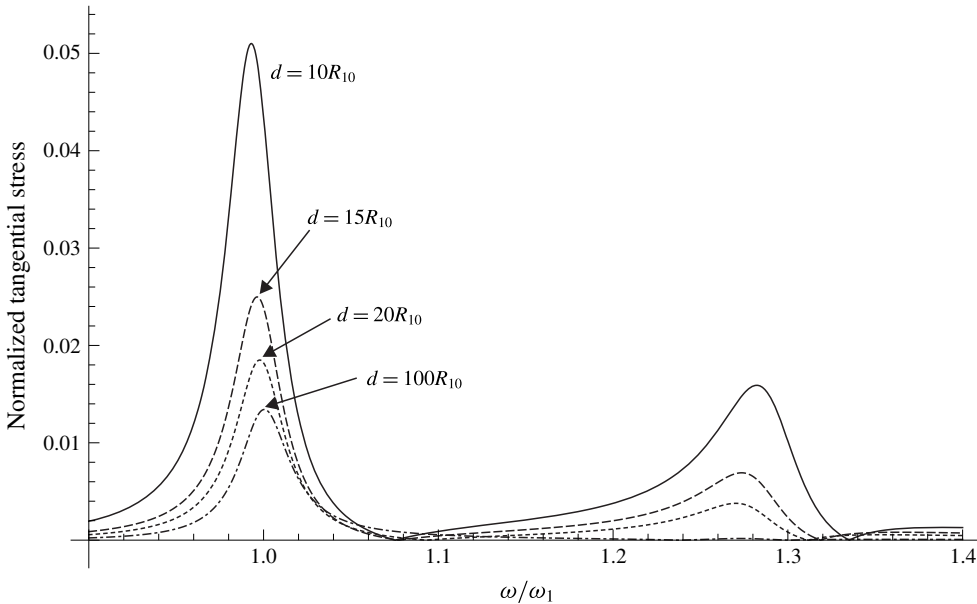
FIGURE 6. Tangential stress for $R_{10} = 5$ µm and $R_{20} = 4$ µm. The other parameters are as in figure 3.

Substituting (2.8) into (2.62) and using (2.15) and (2.16), one finds the radial and tangential components of V_S to be

$$V_{Sr} = V_{Sr1} + V_{Sr2}, \quad V_{S\theta} = V_{S\theta1} + V_{S\theta1}, \tag{2.63a,b}$$

where

$$V_{Srj} = \frac{|A|^2 R_{j0} \cos \theta_j}{2\omega r_j^4} \operatorname{Re} \left\{ i a_j^* \left[\frac{2 b_j R_{j0}^2}{r_j^2} + 2 c_j (k_v r_j h_0^{(1)}(k_v r_j) - h_1^{(1)}(k_v r_j)) \right] \right\}, \tag{2.64}$$

$$V_{S\theta j} = \frac{|A|^2 R_{j0} \sin \theta_j}{2\omega r_j^4} \operatorname{Re} \left\{ i a_j^* \left[\frac{4 b_j R_{j0}^2}{r_j^2} + c_j (2 k_v r_j h_0^{(1)}(k_v r_j) + (k_v^2 r_j^2 - 4) h_1^{(1)}(k_v r_j)) \right] \right\}. \tag{2.65}$$

3. Numerical examples

This section illustrates data that can be obtained using the theory developed in §2. Simulations were made for air bubbles in water with the use of the following physical parameters: $P_0 = 101.3$ kPa, $\rho = 1000$ kg m^{-3}, $\eta = 0.001$ Pa s, $\sigma = 0.072$ N m^{-1}, $c = 1500$ m s^{-1} and $\gamma = 1.4$. It should be mentioned that the experimental verification of the simulated results is presently difficult because necessary experimental data are not available in the literature. We hope that our results will motivate researchers to carry out such experimental measurements.

Figure 2 shows the velocity field of acoustic microstreaming. The calculations were made for bubbles of equal size, $R_{10} = R_{20} = 5$ µm ($\omega_1/2\pi = 724$ kHz), subjected to a plane travelling wave propagating in the positive direction of the axis z. The size
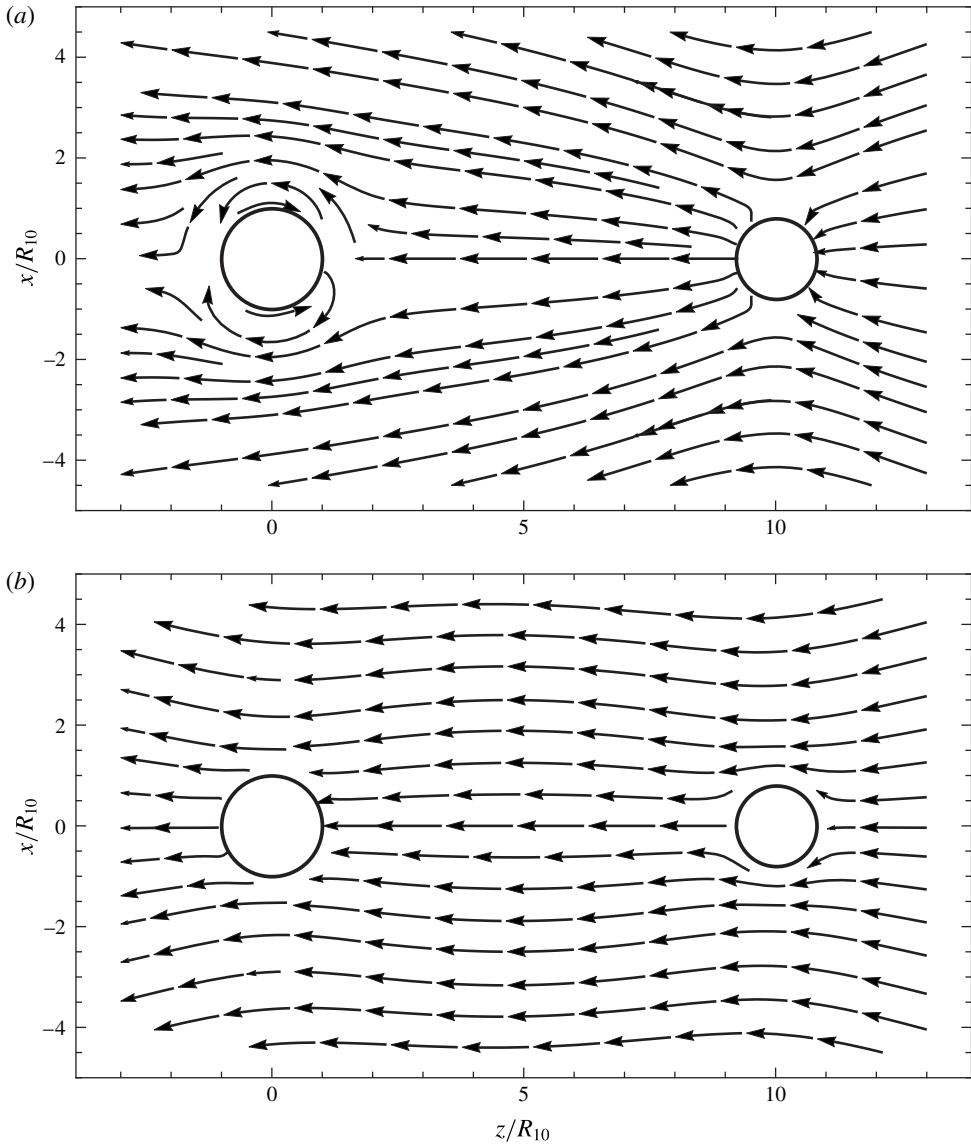
FIGURE 7. Streamlines in the case shown in figure 5. The calculations were made at $d = 10R_{10}$ and the resonance frequencies of the bubbles: (*a*) $0.99\omega_1$ and (*b*) $1.29\omega_1$.

of the bubbles was chosen to be comparable to the size of microbubbles used as contrast agent for echography. The magnitude of the streaming velocity, calculated by (2.52) and (2.53), is shown as a function of the driving frequency ω for different values of the separation distance d at two spatial points, A and B (see figure 1). The coordinates of point A are $z = 0$ and $x = R_{10} + 2\delta_v$, and the coordinates of point B are $z = R_{10} + 2\delta_v$ and $x = 0$. The positions of these points make them representative points for evaluating the tangential and radial components of the velocity field generated by bubble 1. The velocity values are normalized by $|A|^2/(\nu R_{10})$. In a number of applications, such as ultrasonic cleaning and sonoporation, tangential
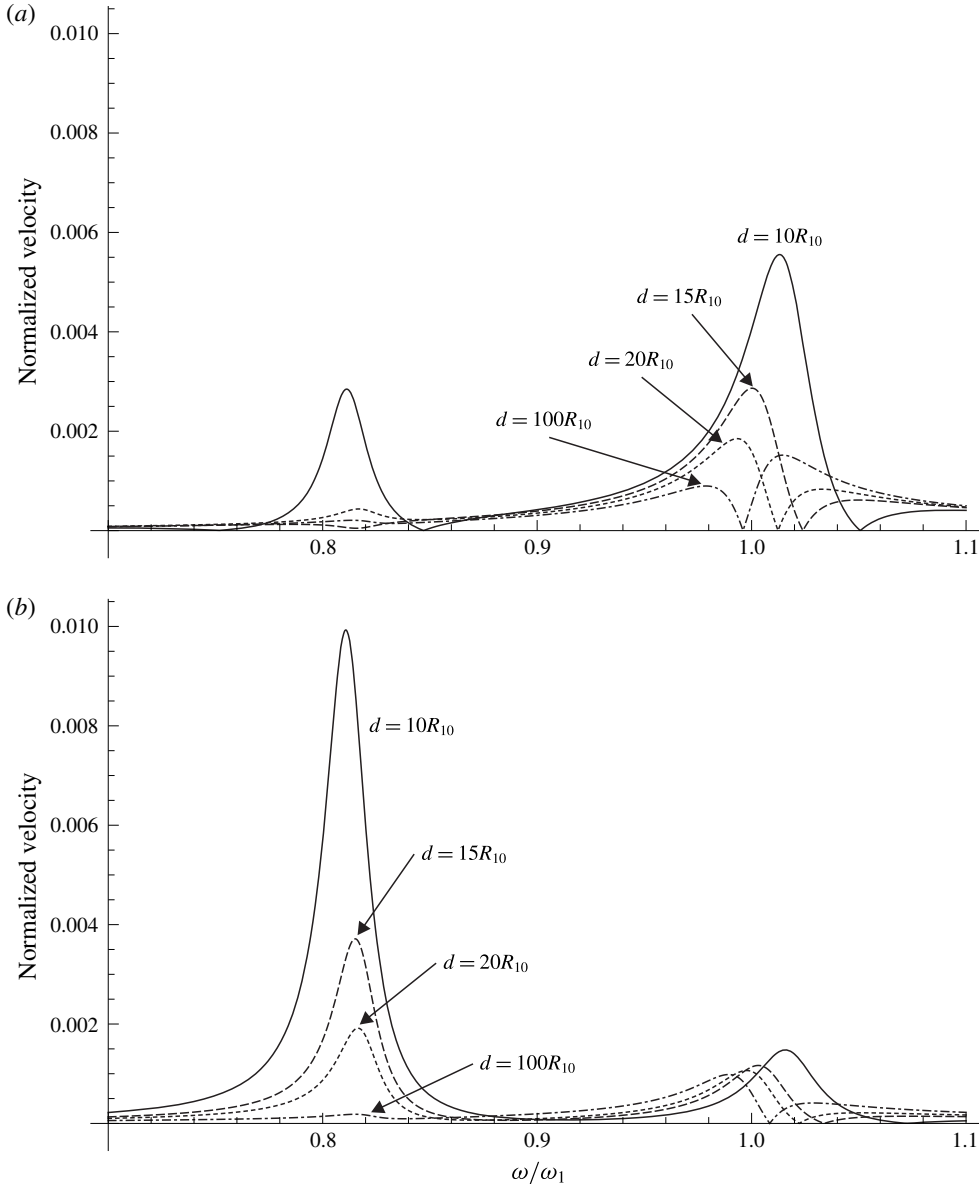
FIGURE 8. Streaming velocity for $R_{10} = 5$ μm and $R_{20} = 6$ μm: (*a*) point A and (*b*) point B. The other parameters are as in figure 2.

stresses produced by acoustic microstreaming are supposed to play an important part. For this reason, we have included figure 3, which depicts the magnitude of the tangential stress at point A and thus illustrates how the interaction of the bubbles affects this characteristic. The stress values are normalized by $\rho|A|^2/(2R_{10}^2)$. As follows from figures 2 and 3, the intensity of the acoustic microstreaming increases considerably with decreasing d when the bubbles are driven near the resonance frequency that they have in the presence of each other ($\approx 0.95\omega_1$). The streamlines of the acoustic microstreaming in the case shown in figure 2 are exemplified by
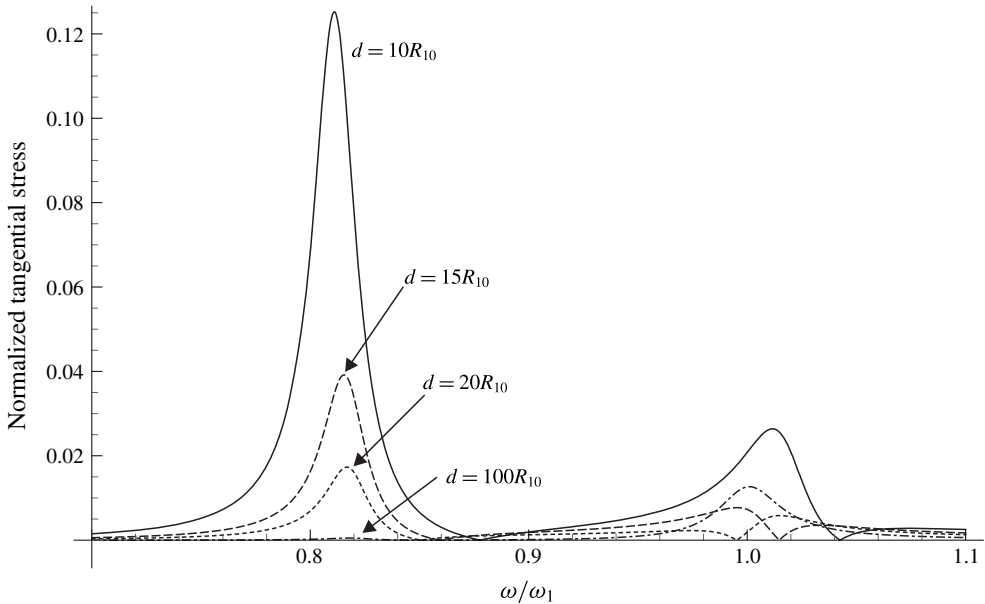
FIGURE 9. Tangential stress for $R_{10} = 5$ μm and $R_{20} = 6$ μm. The other parameters are as in figure 3.

figure 4 at $d = 10R_{10}$ and $\omega = 0.95\omega_1$. As one can see, the streaming pattern is not symmetrical about the x plane midway between the bubbles. This occurs because the liquid translation generated by the incident wave breaks the symmetry of the bubble translational oscillations. Indeed, let us consider (2.32), which gives the translational velocities of the bubbles. This equation shows that the translational velocity of each bubble consists of two contributions. One contribution comes from the scattered field of the neighbouring bubble. It is described by the first term in brackets in (2.32). The bubble velocities caused by this contribution are mirror symmetric in the case of identical bubbles. The second contribution comes from the incident wave. It is described by the second term in brackets in (2.32). The bubble velocities caused by this contribution are equal and therefore the total translational oscillations of the bubbles do not possess mirror symmetry. The symmetry of the streaming pattern appears if the term $R_{j0}\xi_j$ in (2.30)–(2.32) is omitted.

Figures 5–7 demonstrate the case where bubble 1 is bigger than bubble 2: $R_{10} = 5$ μm, $R_{20} = 4$ μm ($\omega_2/2\pi = 925$ kHz). The two main peaks in figure 5 correspond to the resonance frequencies of the bubbles. It is seen that at both frequencies the intensity of the microstreaming is increased considerably with decreasing d. It should be noted, however, that the streaming velocity at point B is shown by figure 5(b) to increase more strongly if the bubbles are driven near the resonance frequency of the smaller bubble (bubble 2). Figure 6 shows the behaviour of the tangential stress at point A, which is seen to be similar to the behaviour of the streaming velocity (cf. figure 5a). Figure 7 displays the pattern of streamlines in the case shown in figure 5. The calculations were made at $d = 10R_{10}$ and the resonance frequencies of the bubbles: (*a*) $0.99\omega_1$ and (*b*) $1.29\omega_1$. As one can see, the streaming pattern in figure 7 is considerably different from that in figure 4, despite the relatively small change in parameters. We suppose that this distinction is related
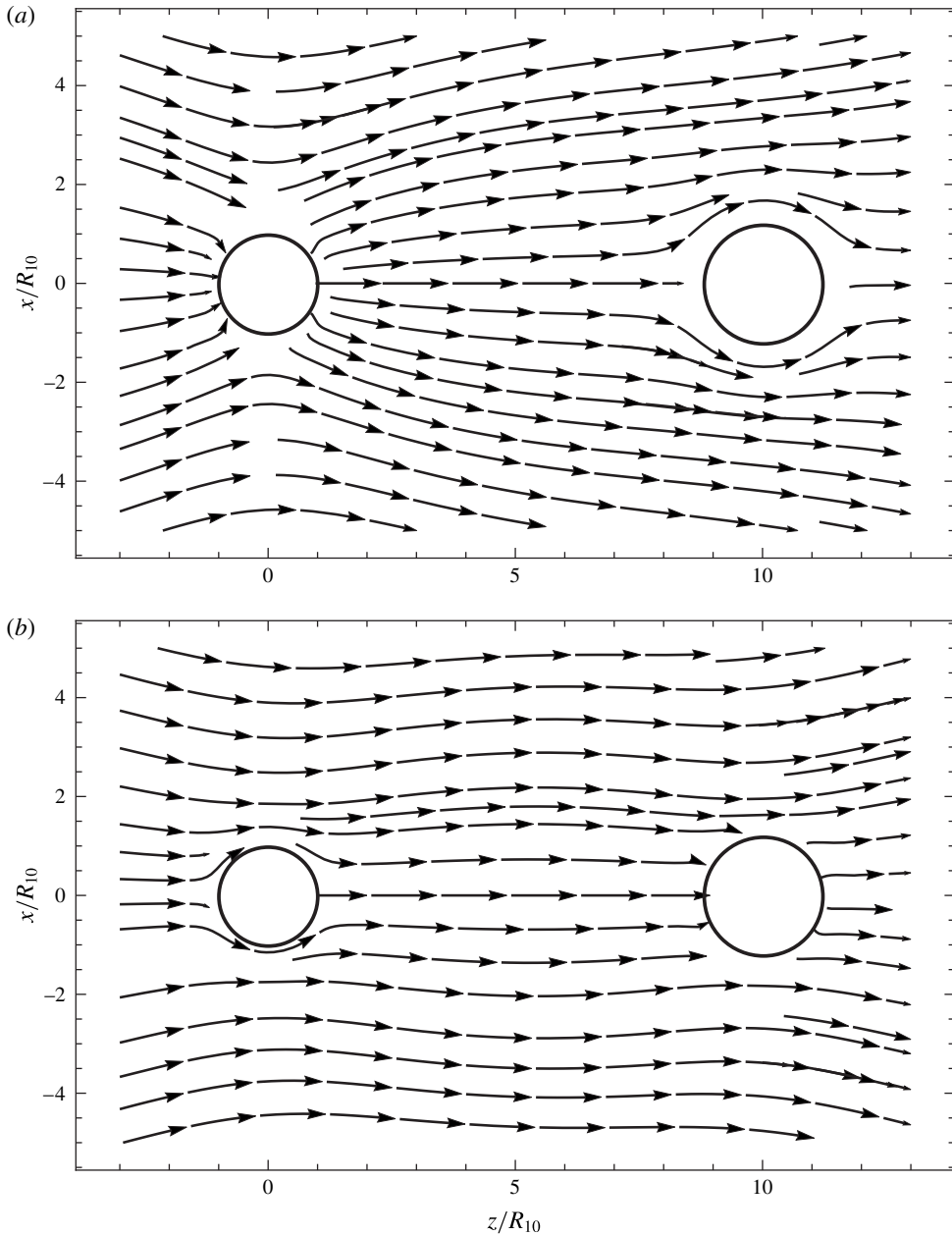
FIGURE 10. Streamlines in the case shown in figure 8. The calculations were made at $d = 10R_{10}$ and the resonance frequencies of the bubbles: (*a*) $0.81\omega_1$ and (*b*) $1.02\omega_1$.

to changes in the phases of the radial and translational oscillations of the bubbles. It has been shown by Longuet-Higgins (1998) and more recently by Doinikov & Bouakaz (2014) that acoustic microstreaming is sensitive to the phase difference between the bubble radial oscillation and the bubble translational velocity. Note also the difference between panels (*a*) and (*b*) in figure 7, which were calculated at different driving frequencies. This difference is explained by the fact that the change
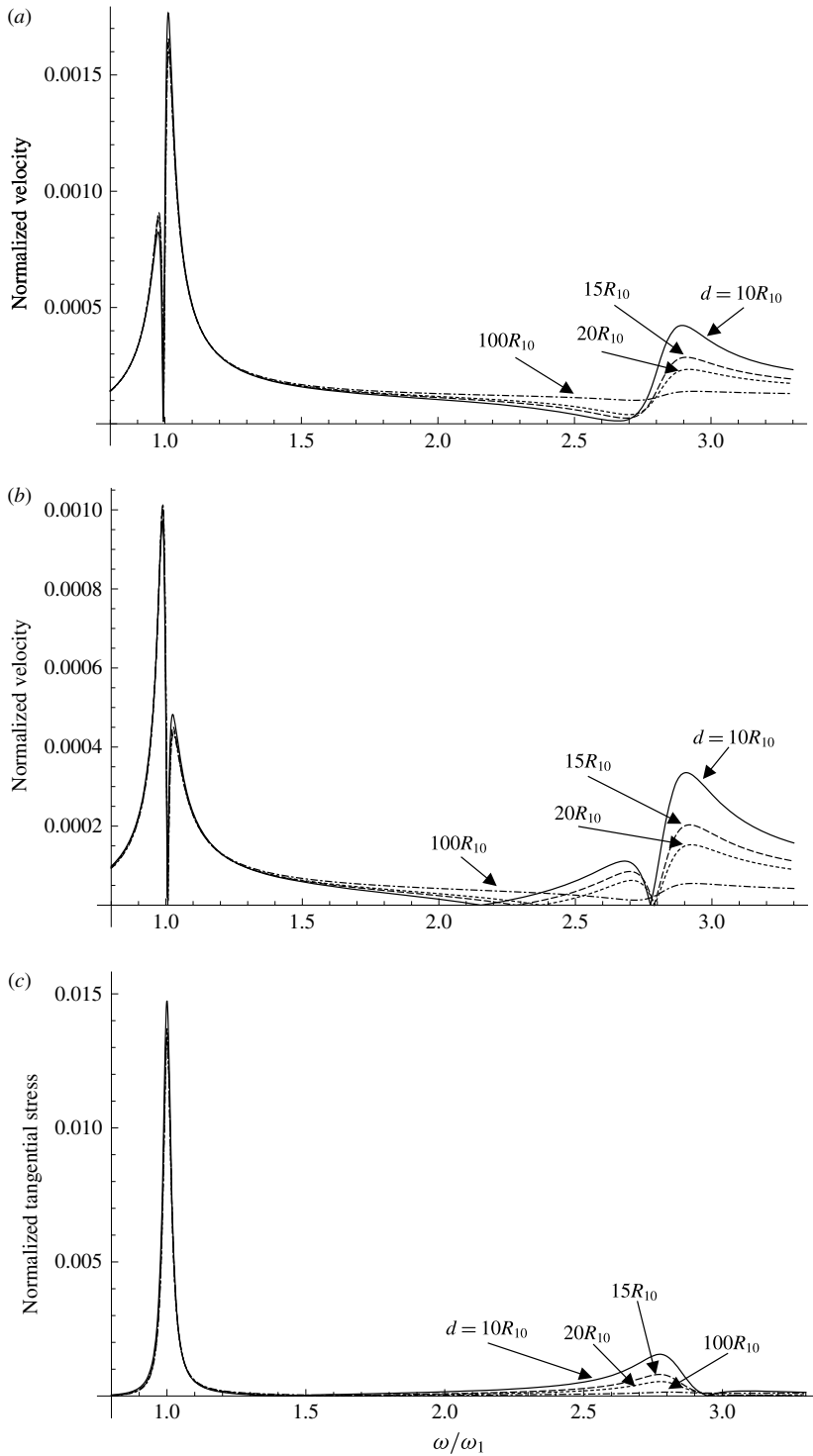
FIGURE 11. Streaming characteristics for $R_{10} = 5$ µm and $R_{20} = 2$ µm: (*a*) point A, (*b*) point B and (*c*) point A. The other parameters are as in figures 2 and 3.
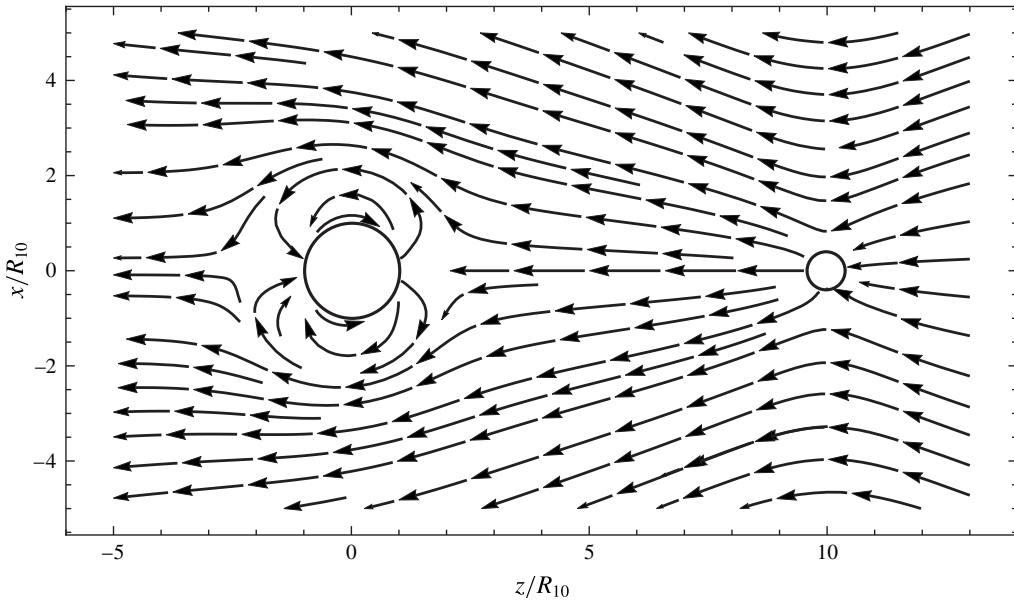
FIGURE 12. Streamlines in the case shown in figure 11 at $d = 10R_{10}$ and $\omega = \omega_1$.

of the frequency leads to changes in both the amplitude and the phase of the bubble radial and translational oscillations (Doinikov & Bouakaz 2014).

Figures 8 and 9 illustrate the case where bubble 1 is smaller than bubble 2: $R_{10} = 5$ μm, $R_{20} = 6$ μm ($\omega_2/2\pi = 594$ kHz). We show this case because the liquid translation generated by the incident wave breaks the symmetry with respect to interchanging bubbles 1 and 2, so this case cannot be obtained from the previous one. As one can see, the streaming velocity at point A increases more strongly if the bubbles are driven near the resonance frequency of the smaller bubble (bubble 1), while the velocity at point B and the tangential stress are increased more strongly near the resonance frequency of the bigger bubble. The pattern of streamlines is presented in figure 10. The calculations were made at $d = 10R_{10}$ and the resonance frequencies of the bubbles: (a) $0.81\omega_1$ and (b) $1.02\omega_1$.

Figures 11 and 12 illustrate the case where there is a considerable difference in bubble sizes: $R_{10} = 5$ μm, $R_{20} = 2$ μm ($\omega_2/2\pi = 2.038$ MHz). The streamlines shown in figure 12 were calculated at $d = 10R_{10}$ and $\omega = \omega_1$. Comparison with the results obtained by Longuet-Higgins (1998) for a single bubble in an infinite liquid shows that, despite the great difference in bubble sizes, the influence of the bubble interaction on acoustic microstreaming remains significant on condition that d is not large.

The developed theory can also be applied to the case of a bubble near a rigid wall. In our previous paper (Doinikov & Bouakaz 2014), the effect of a rigid wall on microstreaming in the immediate vicinity of the bubble surface was studied. Microstreaming in the bulk liquid between the bubble and the boundary layer at the wall was not considered and the liquid velocity caused by the primary incident wave was neglected. These shortcomings are overcome in the present theory. To describe the presence of a wall, bubble 2 should be treated as a mirror bubble, assuming the wall to be at the distance $d/2$ from bubble 1. In this case, the velocity potential of the standing wave caused by the wall can be written as $\varphi_I = A \exp(-i\omega t) \cos(k(z - d/2))$, assuming bubble 1 to be at $z = 0$. It follows that $\xi_1 = k \sin(kd/2)$ and ξ_2 should be
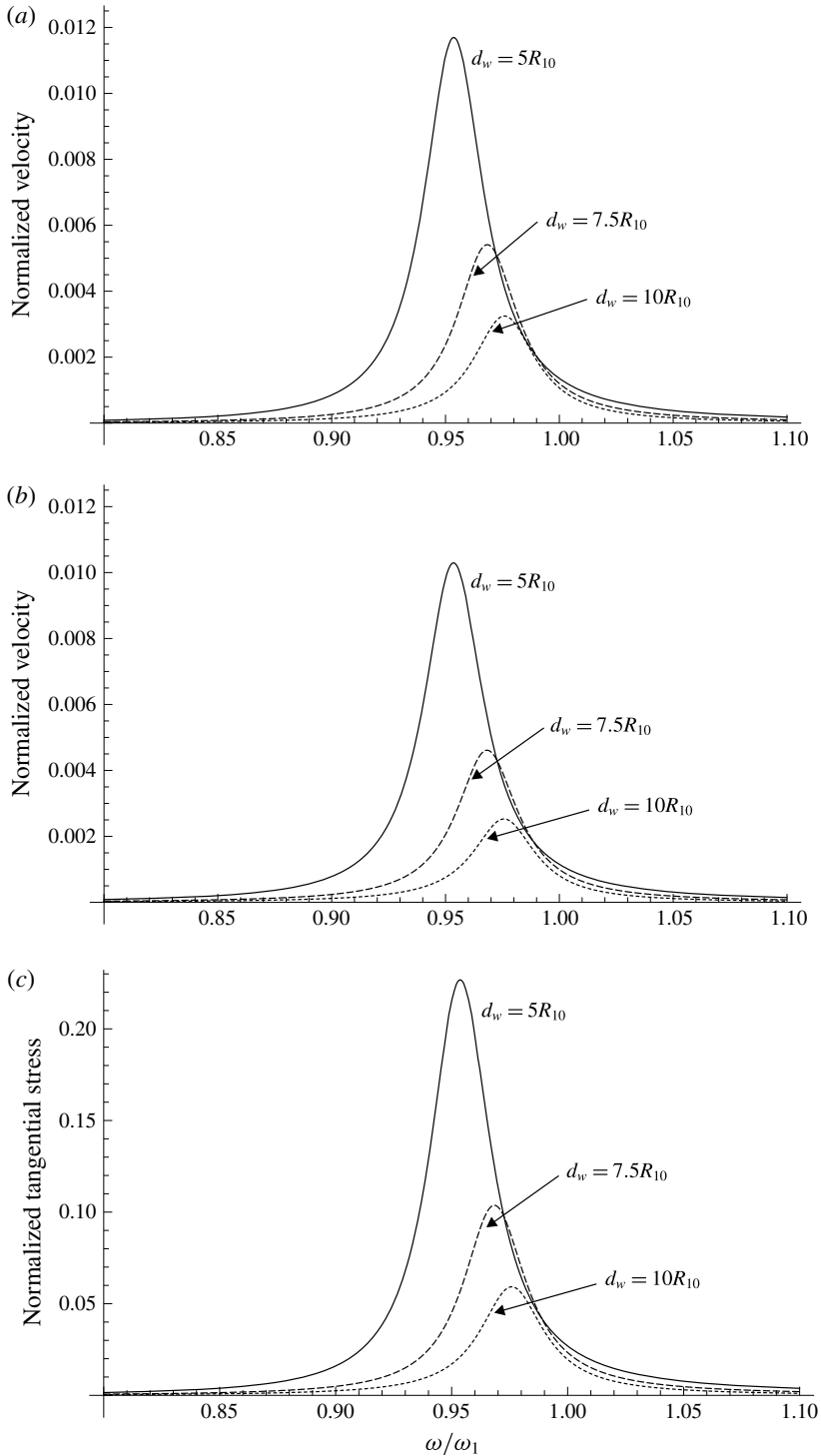
FIGURE 13. Streaming characteristics for a bubble with $R_{10} = 5$ µm in the presence of a rigid wall: (a) velocity at point A, (b) velocity at point B, and (c) tangential stress at point A.
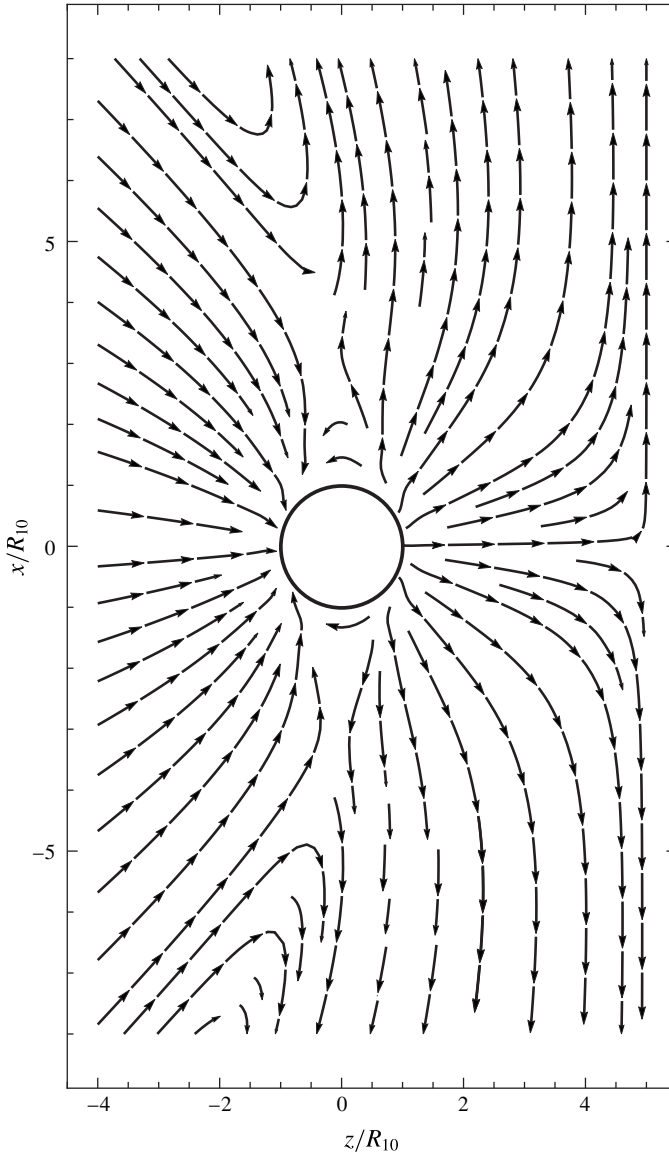
FIGURE 14. Streamlines in the case shown in figure 13 at $d_w = 5R_{10}$ and $\omega = 0.95\omega_1$. The wall is to the right of the bubble.

set to be equal to $-\xi_1$ to provide mirror symmetry. The behaviour of microstreaming is exemplified by figure 13, where $R_{10} = 5$ µm and $d_w = d/2$ is the distance between the bubble and the wall. As one would expect, the intensity of the microstreaming is increased considerably with decreasing d_w if the bubble is driven near the resonance frequency that it has in the presence of the wall. Figure 14 shows the pattern of streamlines at $d_w = 5R_{10}$ and $\omega = 0.95\omega_1$, the wall being to the right of the bubble.

There is one point to be made. Our theory does not impose explicit limitations on the amplitude of the bubble translational velocity and hence on the amplitude of the bubble translational displacement. However, it has been pointed out by

Longuet-Higgins (1998) that the approximation approach that he used to calculate streaming, and whose principles we follow in our study, is valid only if the translational displacement is small compared to the bubble radius, although it does not need to be small compared to the thickness of the viscous layer at the bubble surface. As mentioned in his work, this condition is met in many applications. In our previous paper (Doinikov & Bouakaz 2014), we also demonstrate by particular examples that this condition is satisfied in many cases of interest.

4. Conclusion

Analytical equations have been derived that describe acoustic microstreaming generated by two interacting gas bubbles undergoing small radial and translational oscillations in an acoustic field. Numerical simulations were performed to compare the characteristics of acoustic microstreaming at different frequencies, separation distances between the bubbles and bubble sizes. It was shown that the interaction of the bubbles leads to a considerable increase in the intensity of the velocity and stress fields of acoustic microstreaming if the bubbles are driven near the resonance frequencies that they have in the presence of each other. Examples of streamlines for different situations were presented. It was also demonstrated that the developed theory could be applied to the case of a bubble near a rigid wall.

Acknowledgement

REFERENCES

ABRAMOWITZ, M. & STEGUN, I. A. 1972 *Handbook of Mathematical Functions*. Dover.

COLLIS, J., MANASSEH, R., LIOVIC, P., THO, P., OOI, A., PETKOVIC-DURAN, K. & ZHU, Y. 2010 Cavitation microstreaming and stress fields created by microbubbles. *Ultrasonics* **50**, 273–279.

DAVIDSON, B. J. & RILEY, N. 1971 Cavitation microstreaming. *J. Sound Vib.* **15**, 217–233.

DOINIKOV, A. A. & BOUAKAZ, A. 2010*a* Acoustic microstreaming around a gas bubble. *J. Acoust. Soc. Am.* **127**, 703–709.

DOINIKOV, A. A. & BOUAKAZ, A. 2010*b* Acoustic microstreaming around an encapsulated particle. *J. Acoust. Soc. Am.* **127**, 1218–1227.

DOINIKOV, A. A. & BOUAKAZ, A. 2014 Effect of a distant rigid wall on microstreaming generated by an acoustically driven gas bubble. *J. Fluid Mech.* **742**, 425–445.

ELDER, S. A. 1959 Cavitation microstreaming. *J. Acoust. Soc. Am.* **31**, 54–64.

KOLB, J. & NYBORG, W. 1956 Small-scale acoustic streaming in liquids. *J. Acoust. Soc. Am.* **28**, 1237–1242.

LIGHTHILL, S. J. 1978 Acoustic streaming. *J. Sound Vib.* **61**, 391–418.

LIU, R. H., YANG, J., PINDERA, M. Z., ATHAVALE, M. & GRODZINSKI, P. 2002 Bubble-induced acoustic micromixing. *Lab on a Chip* **2**, 151–157.

LIU, X. & WU, J. 2009 Acoustic microstreaming around an isolated encapsulated microbubble. *J. Acoust. Soc. Am.* **125**, 1319–1330.

LONGUET-HIGGINS, M. S. 1998 Viscous streaming from an oscillating spherical bubble. *Proc. R. Soc. Lond.* A **454**, 725–742.

MAKSIMOV, A. O. 2007 Viscous streaming from surface waves on the wall of acoustically-driven gas bubbles. *Eur. J. Mech. (B/Fluids)* **26**, 28–42.

NYBORG, W. L. 1958 Acoustic streaming near a boundary. *J. Acoust. Soc. Am.* **30**, 329–339.

NYBORG, W. L. 1965 Acoustic streaming. In *Physical Acoustics* (ed. W. P. Mason), vol. 2B, pp. 265–330. Academic.

NYBORG, W. L. 1978 Physical principles of ultrasound. In *Ultrasound: Its Applications in Medicine and Biology* (ed. F. J. Fry), pp. 1–75. Elsevier.

ROONEY, J. A. 1970 Hemolysis near an ultrasonically pulsating gas bubble. *Science* **169**, 869–871.

ROONEY, J. A. 1972 Shear as a mechanism for sonically induced biological effects. *J. Acoust. Soc. Am.* **52**, 1718–1724.

THO, P., MANASSEH, R. & OOI, A. 2007 Cavitation microstreaming in single and multiple bubble systems. *J. Fluid Mech.* **576**, 191–233.

WANG, C., JALIKOP, S. V. & HILGENFELDT, S. 2012 Efficient manipulation of microparticles in bubble streaming flows. *Biomicrofluidics* **6**, 012801.

WU, J. 2002 Theoretical study on shear stress generated by microstreaming surrounding contrast agents attached to living cells. *Ultrasound Med. Biol.* **28**, 125–129.

WU, J. & DU, G. 1997 Streaming generated by a bubble in an ultrasound field. *J. Acoust. Soc. Am.* **101**, 1899–1907.

WU, J. & NYBORG, W. L. 2008 Ultrasound, cavitation bubbles and their interaction with cells. *Adv. Drug Deliv. Rev.* **60**, 1103–1116.